Ion implantation for silicon solar cells

Henry Hieslmair, **Ian Latchford**, **Lisa Mandrell**, **Moon Chun** & **Babak Adibi**, Intevac, Santa Clara, California, USA

ABSTRACT

This paper presents the background and technology development of the use of ion implantation technology in today's crystalline silicon solar cell manufacturing lines. The recent history of ion implantation development and commercialization is summarized, and an explanation is given for the cell efficiency improvements realized using the technique on p-type mono-crystalline cells. The potential economic impact on the factory is also discussed.

Introduction

There are continuing pressures on PV manufacturers to lower manufacturing costs further while increasing efficiency. The efficiency of the module impacts all downstream area-related costs in the installed PV system, such as wiring and bracing structures. Manufacturers have already brought costs down to very low levels through better yield and economies of scale, and are now evaluating various approaches to improving cell efficiency. While standard screen-printed p-type cell efficiency can still be improved, most roadmaps will transition to advanced cell designs to meet the increased efficiency requirements. Thus, any investment in near-term manufacturing solutions has to also offer extendibility paths towards advanced cells and materials. There are numerous high-efficiency device architectures and various technology roadmaps regarding material type, cell architecture, process flow and process equipment. Cell efficiencies are generally predicted to improve as shown in Fig. 1, with the implication that new designs and processes will be adopted by industry to achieve the higher efficiencies.

> "Ion implantation has a unique characteristic in that it is both beneficial to current cell designs and extendible to future cell architectures."

Ion implantation has a unique characteristic in that it is both beneficial to current cell designs and extendible to future cell architectures. In the near term, ion implantation provides higher cell efficiency for P emitters, narrower efficiency distribution and a lower overall cost. Equally important, the manufacturing of many advanced device designs can be significantly simplified by ion implantation. Recent efforts to commercialize high-productivity ion implanters have placed ion implantation technology centre stage in the silicon PV roadmap.

Synopsis of implantation used in solar cells

Throughout the history of implanted solar cells, various implanter tool designs have been utilized, the two main ones being *mass-analyzed* and *non-mass-analyzed*. Mass analysis is performed with a large magnet which bends the ion beam through an aperture. Only species with the proper mass and energy pass through the aperture. The filtered ion beam current is typically significantly less than the initial ion beam current. Non-mass-analyzed implanters, however, feature higher beam currents and lower capital costs, although they exhibit a broad range of ion energies and may co-implant other precursor species such as H+ and F+. Ion sources have also changed over the decades and include glow discharge, microwave and inductively coupled RF plasmas. One of the earliest references to using ion implantation for solar cells was in 1964 by King and Burrill [2], who used a Van de Graaff electrostatic accelerator to accelerate boron or phosphorus ions generated by a microwave ion source.

Glow discharge plasma source designs were common in the 1970s and 1980s [3–6]. A variety of dopant gases – including BF_3, B_2H_6, PH_3 and PF_5 – were utilized as the precursors. One of the most advanced and ambitious implementations of implantation for solar cells was that of the Hoxan Corporation in Japan in 1982 [7]. Using 4" round wafers, Hoxan built an integrated, in-line, computer-controlled, 9MW manufacturing line with a non-mass-analyzed implanter using BF_3 (40keV) to form the rear boron back-surface field (B-BSF), and a second non-mass-analyzed implanter utilizing vapours from a heated solid P source (25keV) to form the emitter. Annealing was performed with a halogen lamp and followed by TiO_2 ARC and screen printing/firing stages. The entire automated manufacturing line also included tabbing and stringing and then module assembly and lamination. Each process was synchronized to five seconds per wafer for a throughput of 720 wafers per hour (wph).

Also in the 1980s, several researchers utilized commercial mass-analyzed beamline implanters for solar cells. Mass-analyzed ion implantation was becoming more important for integrated-circuit applications, in which the energy precision was crucial. Spitzer et al. [8–10] investigated various implantation conditions and anneals for both phosphorus and boron emitters using mass-analyzed implantation; for phosphorus emitters, 18% efficiencies were obtained.

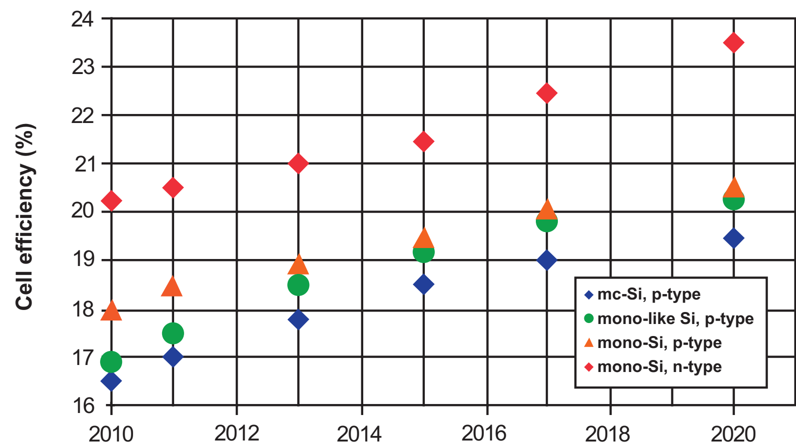

Figure 1. ITRPV Roadmap, March 2012 update: stabilized cell efficiency trend curves [1].

Later, in 1987, using a glow discharge source, Wood et al. [11] demonstrated 19.5% efficiency (AM1.5) using a non-mass-analyzed B_2H_6 (5% in H_2) implant for the emitter (n-type wafer), and non-mass-analyzed PH_3 (1% in H_2) implant for the phosphorus back-surface field (P-BSF). Using oxide passivation and photolithography to pattern evaporated metal contacts, a V_{oc} greater than 660mV was demonstrated. The high V_{oc} obtained demonstrates the exceptional quality of the implanted emitter and BSF, and indicates that the co-implanted hydrogen was not deleterious, despite the dilution of the dopant gas in H_2.

More recently, numerous groups have shown high cell efficiencies on industrial phosphorus emitter cells using modern commercial mass-analyzed implanters. For example, Suniva Inc. has demonstrated high cell efficiencies of ~19% on an industrial scale using a mass-analyzed ion implanter [12,13]. Non-mass-analyzed implanters have also been targeting solar cell applications. For instance, Intevac has demonstrated a continuous flux non-mass-analyzed implant tool – ENERG*i*™ – specifically designed for the solar industry, featuring a 2400wph throughput, sheet resistance uniformities of 1% (σ/mean) wafer to wafer, and a cost of ownership (COO) that is competitive with the standard $POCl_3$ diffusion process. In collaboration with China Sunergy, Intevac has achieved high efficiencies of 19% in an industrial line [14] using the ENERG*i* implanter.

Advantages of ion implantation

Ion implantation in general provides numerous process advantages. Specifically, the advantages of implantation include:

- High-precision dopant doses and profiles
- High uniformity and repeatability
- Single-sided doping capability
- Boron-doping capability
- Patterned doping

For today's standard screen-printed p-type cells, ion implantation yields improved efficiencies through precision phosphorus profiles and high uniformity. The single-sided doping capability simplifies the process flow by eliminating the need for phosphosilicate glass (PSG) removal and edge isolation. Additionally, in situ thin passivating oxides can be easily incorporated during the subsequent anneal. Single-sided ion implantation can benefit thinner wafers by substituting a high-stress alloyed Al-BSF with B-BSF.

Tools and technologies adopted for today's processes must also be extendible and compatible with the future cell designs throughout a manufacturer's development roadmap. With the advent of industrial processes to passivate p-type surfaces, there is increasing benefit in transitioning away from standard cell structures with an aluminium-alloyed BSF. The single-sided doping capability of implantation facilitates this transition by eliminating multiple diffusion-barrier formation and removal steps otherwise required by furnace diffusions to form a B-BSF or P-BSF.

Patterned doping for selective emitters can be accomplished through inserting a shadow mask into the ion beam [15,16]. The ENERG*i* ion implantation can also pattern dopants for selective emitters by using shadow masks so that both the blanket and SE dopants are implanted in the same single-wafer pass through the ion beam.

Because boron diffusion has been difficult to implement cost-effectively in industry, implanting both phosphorus and boron, followed by a single co-anneal, greatly simplifies many designs, such as passivated rear cell designs [13,17,18] and n-type cells with boron emitters [19–22]. For very high efficiencies, ion implantation holds the promise of significant process simplification for interdigitated back-contact (IBC) cells [23–25]. Patterned, single-sided P and B doping with a co-anneal has the potential to make IBC manufacturing far simpler than using repeated diffusion masks and furnace diffusions, as shown in Fig. 2. This comparison of a furnace-based IBC process flow and an implant-based process

The Efficient Alternative You Wanted!

Merck's printable etchants for advanced patterning for

- Selective Emitter
- MWT (Metal Wrap Through)
- LBSF (Local Back Surface Field)

Easy, fast and environmentally friendly

www.merck-performance-materials.com www.isishape.com

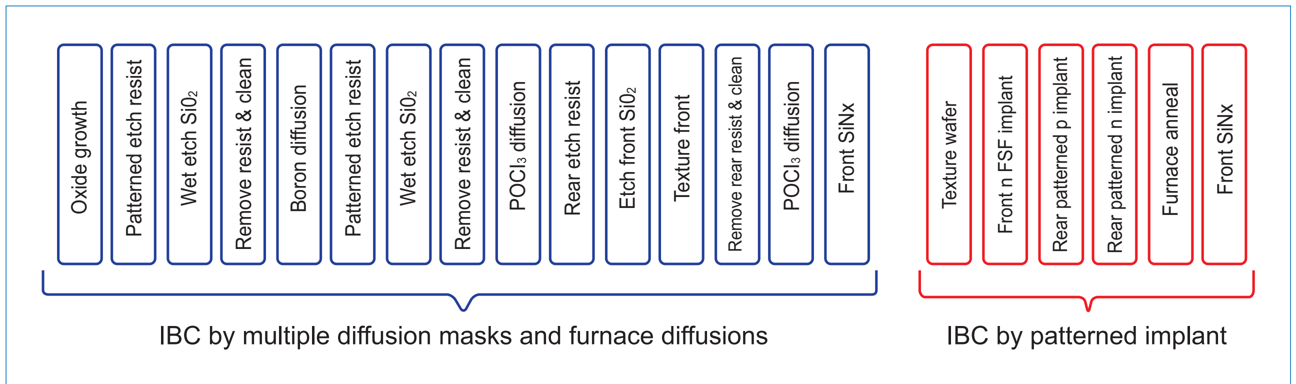

Figure 2. Comparison of process flows for IBC cells by diffusion and by patterned implantation.

flow illustrates the potential process simplification using implantation.

Defect engineering synopsis

Ion implantation damage and recrystallization has been studied for decades. Consequently, very sophisticated models of damage formation and annealing exist, which are beyond the scope of this paper, but a brief synopsis of relevant damage and annealing processes will be given. For phosphorus implantation, the strategy is to form an amorphized surface layer which recrystallizes epitaxially with very few defects during a subsequent higher temperature annealing step. This process is called solid-phase epitaxial regrowth (SPER). The key to minimizing defects through the SPER process is to form a fully amorphized layer with a smooth α/c interface and a minimum of damage beyond the α/c interface. While phosphorus implantation does amorphize the silicon well, boron implantation is more complicated because it does not typically amorphize the top layer of silicon for the doses desired for solar cells.

Except for the lightest elements such as H, as the impinging ion enters the silicon, it transfers most of its energy to the target lattice through collisions. These collisions create local heat and, if more than 15–20eV is transferred to the lattice silicon atoms, one or more Frenkel pairs (Si vacancy + Si interstitial) are created [26]. The damage along the path of the impinging ion, i.e. the collision cascade, is highest near the end of the range where the ion's velocity is sufficiently slow so that nearly every atomic interaction results in a displacement event. Some of the created defects have a very short lifetime, and, with the localized heating assisting the defect mobility, the defects can begin to annihilate (i.e. anneal) on a nanosecond timescale. This dynamic annealing is undesirable because, as mentioned earlier, a well-formed amorphous layer requires significant damage accumulation. Partially amorphized layers or regions with sub-amorphous damage do not typically result in low defects, even after higher temperature annealing. Dynamic annealing can be prevented by cooling the sample to cryogenic temperatures. Implantation studies at such low temperatures illustrate the strong effects of dynamic annealing at higher temperatures. For example, the minimum dose required to amorphize at −150°C is less than 1×10^{15} B/cm^2. In contrast, at room temperature the required implantation dose is ~2×10^{16} B/cm^2 for amorphization.

Other factors contributing to better amorphization include ion species, continuous flux and dose rate [27]. Heavier ions, such as phosphorus, create more damage per ion and therefore require lower doses for full amorphization. Viewing the amorphization process as a dynamic competition between damage accumulation and dynamic annealing, one can understand that a higher dose rate [28] and continuous implant will accumulate damage faster and help form fully amorphized layers. Numerous ion implantation tools raster or pulse the ion beam, thus allowing time between the beam sweeps for dynamic annealing to occur. On the other hand, continuous fluxes and higher dose rates are expected to result in deeper amorphous layers, with less sub-amorphous damage beyond the α/c interface.

During a subsequent annealing step, the amorphous layers will recrystallize epitaxially, with the α/c interface moving towards the surface at a few hundred nm/s at 700°C [29]. Typically, the recrystallization is fully complete by the time the wafer boat is loaded into a furnace at 700°C. Dopants within this regrown epitaxial layer have high levels of activation, even if the dopant concentration somewhat exceeds the solubility during the SPER [30]. However, during the anneal (typically >800°C), equilibrium concentrations will be restored and supersaturated dopants will precipitate or cluster [31]. Thus proper implant and anneal optimization is important for obtaining emitters of the highest efficiency. Additionally, during the anneal the minor sub-amorphization damage, which lies deeper than the initial α/c interface, can be minimized or completely annealed as the phosphorus diffuses deeper into the silicon.

The ENERG*i* implantation tool was designed with both the needs of the solar market and defect-free emitters in mind. The ENERG*i* tool cools the wafer, which undergoes a single pass through a continuous and high-flux phosphorus ion beam. The difference between a rastered and a continuous flux implantation is schematically illustrated in Fig. 3 for the same total dose (area of each coloured region). At any given point on a silicon wafer, the rastered ion beam allows periods of time for dynamic annealing to occur and may result in poorer amorphized layers.

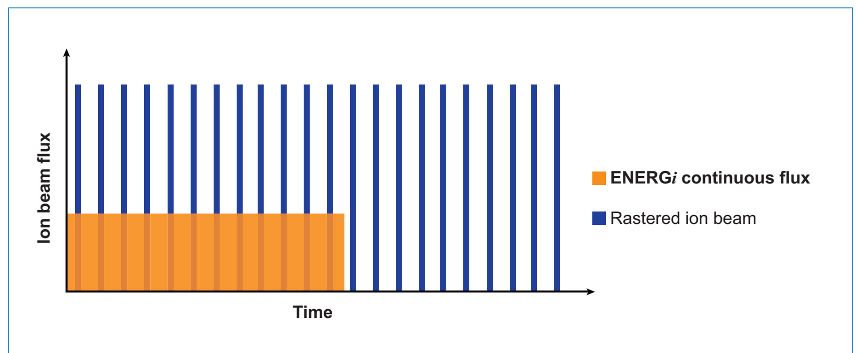

Figure 3. The ion beam flux observed for any given point on a wafer for a rastered ion beam and for a continuous flux ENERG*i* ion beam for the same dose (area of each coloured region).

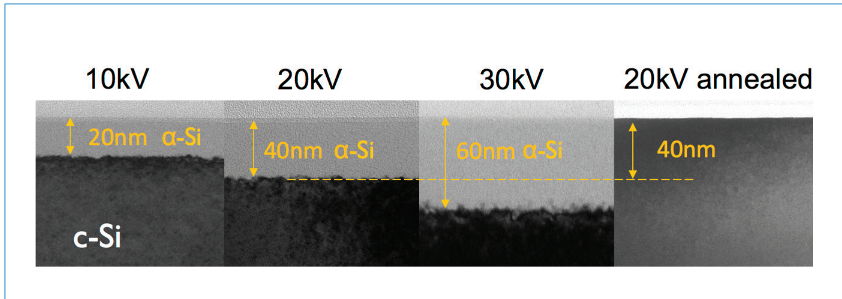

Figure 4. Transmission electron microscope (TEM) images of ENERG*i* implanted samples, showing amorphization at 10kV, 20kV and 30kV. Also shown is the defect-free recrystallization of the 20kV implanted sample.

At Intevac, fully amorphized layers with doses as low as 1×10^{15} P/cm^2 have been demonstrated. Examples of amorphization at different energies using the ENERG*i* continuous-flux implantation tool are shown in Fig. 4, as well as the defect-free recrystallization of the 20kV implanted sample.

Boron does not amorphize silicon at doses of interest for solar cells. Instead of SPER, the sub-amorphous implant damage needs to be annealed at higher temperatures. Good emitters have been demonstrated by annealing at high temperatures such as 1000°C. Some problems with V_{oc} or internal quantum efficiency (IQE) response have been reported for B+ implanted emitters despite low J_{0E} values having been achieved [32–34]. However, other studies have shown excellent results with similar B+ implanted emitters [21,22]. To be successful, boron implantation for solar cells will depend on the right tool, implant and anneal.

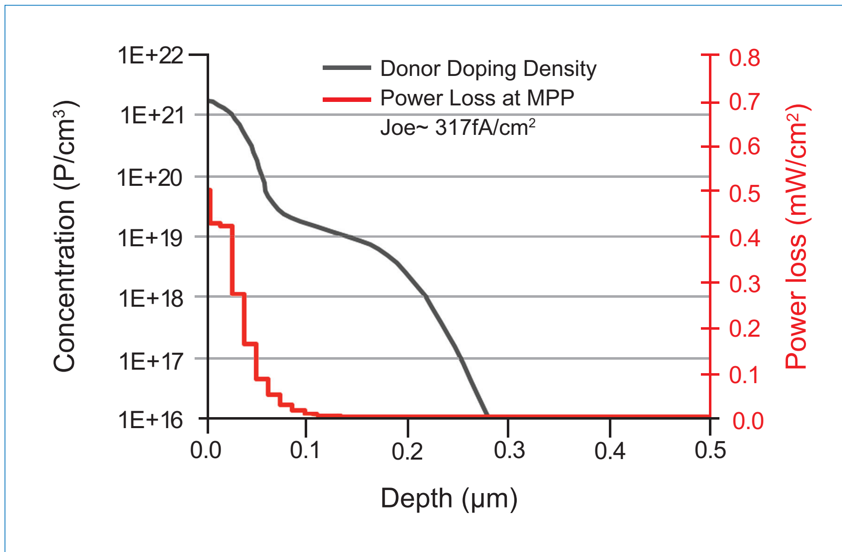

Figure 5. PC1D simulation illustrating typical power losses due to high phosphorus concentrations in the near-surface region (<50nm).

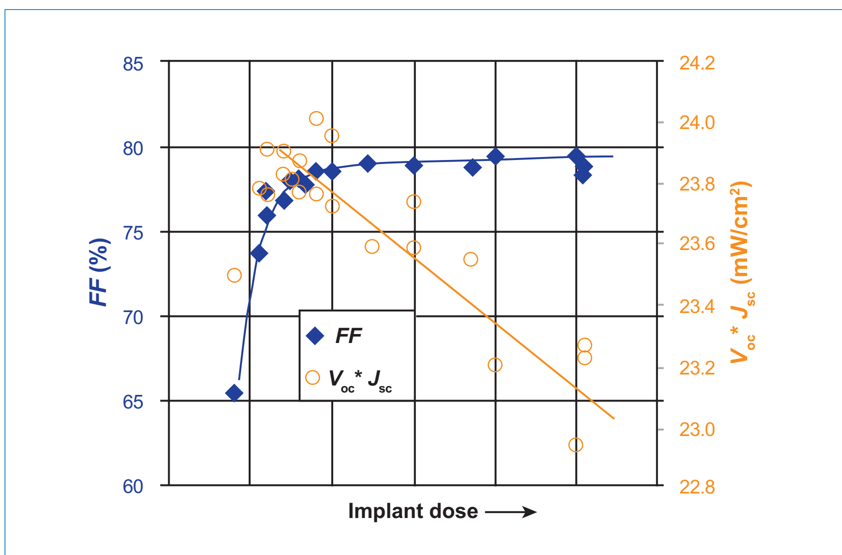

Figure 6. The effect of implanted phosphorus dose on *FF*, V_{oc} and J_{sc}. At lower phosphorus implant doses, V_{oc} and J_{sc} improve, whereas *FF* degrades abruptly.

Efficiency improvements for standard P emitters by ion implantation

The efficiency gain from ion implantation in today's phosphorus emitters is based on precisely controlling the near-surface phosphorus dose. Any phosphorus emitter optimization entails maximizing the sheet resistance while minimizing carrier recombination and contact resistance to the front metallization. While the sheet resistance is a function of the entire profile shape, the recombination and the contact resistance are very sensitive to the portions of the emitter containing the highest concentration of phosphorus, i.e. the first ~50nm of the emitter. Fig. 5 shows a PC1D simulation, illustrating the general importance of the near-surface region. The black curve indicates the phosphorus profile, with concentration values on the left axis; the red curve is an approximation of the power loss (as a function of depth) caused by carrier recombination. (Fig. 5 is intended only to illustrate the importance of the near-surface region – various assumptions and simplifications were made that are outside the scope of this paper.)

By lowering the near-surface phosphorus dose, improved emitters and higher efficiency cells can be fabricated. An improvement in V_{oc} and J_{sc} with decreasing dose is shown in the data plotted in Fig. 6: as the total phosphorus dose is decreased, recombination in the emitter is reduced, which results in improved V_{oc} and J_{sc}.

However, below a threshold phosphorus dose the contact resistance to the front metallization may increase significantly. The industrial Ag-based screen-printed metallization requires high (degenerate) doping levels at the Ag-Si interface in order to make low-resistance tunnelling junctions [35]. This effect places a lower limit on the reduction of the near-surface phosphorus dose. In Fig. 6, the fill factor (*FF*) is also plotted as a function of implanted phosphorus dose. For a fixed anneal, the near-surface dose will be proportional to the total implanted dose. Below a threshold dose, the paste and firing conditions result in higher contact resistance and degraded *FF*. While new pastes are able to contact lower surface concentrations, a strong drop in *FF* will still occur if the concentration is too low. Thus, for industrial high-efficiency emitters the near-surface phosphorus dose

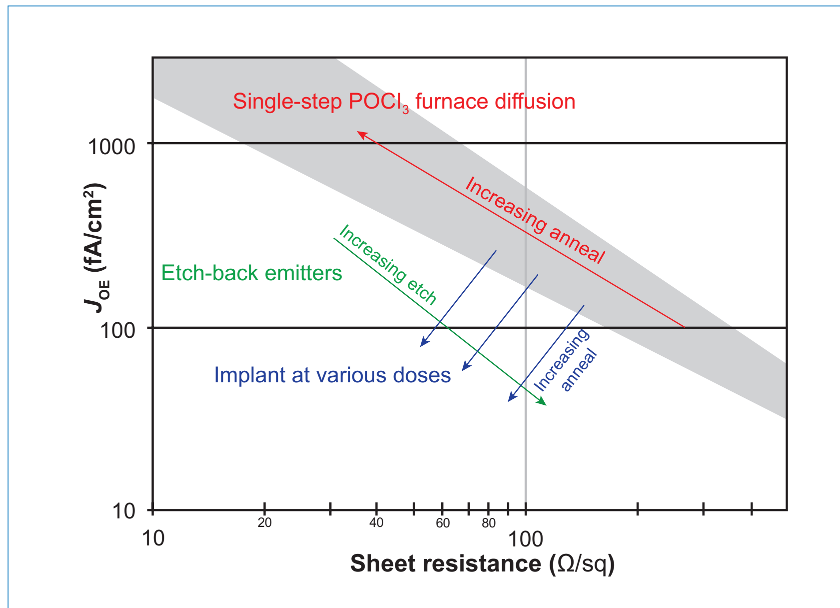

Figure 7. Process trajectories for various emitter formation techniques.

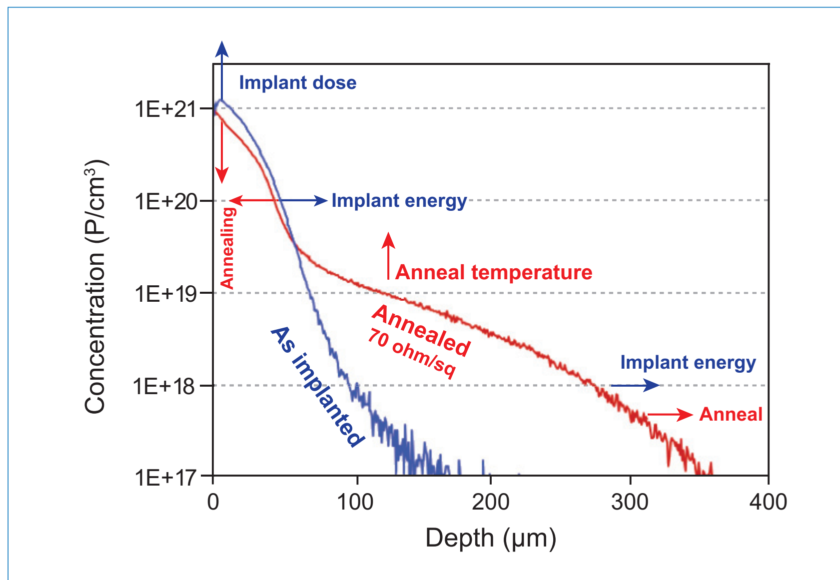

Figure 8. Impacts of various implant and anneal parameters for tailoring P profiles.

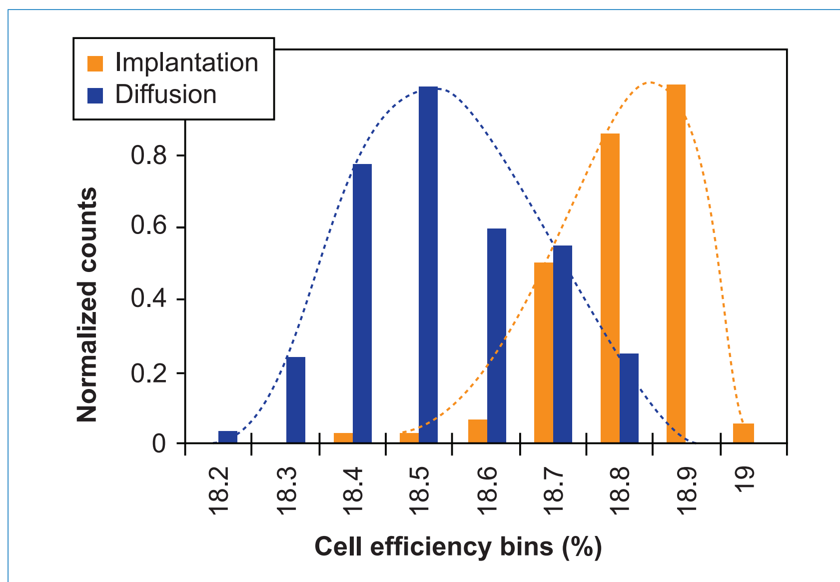

Figure 9. Comparison of industrial cells made by $POCl_3$ diffusion and ion implantation.

must be precisely optimized and controlled across the wafer and from wafer to wafer.

Such near-surface phosphorus dose control is more difficult with $POCl_3$ diffusion. In this case the phosphorus dose *and* phosphorus drive-in are increasing during the anneal. The near-surface dose is very sensitive to temperature and ambient gas variations in the furnace. This process trajectory (increase in dose and J_{0E} with reduction in sheet resistance) is illustrated in Fig. 7 by the red arrow. More complex furnace recipes involving multiple anneal plateaus and ambient gases [9] can, to a limited extent, alter the near-surface phosphorus concentration and improve J_{0E}. The $POCl_3$ process is therefore depicted as a wider range by the grey area in Fig. 7; for illustration purposes, the emitter etch-back [36] process trajectory is also included and is indicated by the green arrow. During the etch-back, the surface and peak concentrations are reduced, resulting in a lower J_{0E} emitter and higher sheet resistance.

In contrast, the ion implantation process separates the dose step and the drive-in step in order to precisely control and tailor the final phosphorus profile. During the anneal, the as-implanted phosphorus dopant starts to diffuse into the silicon. This redistribution of the implanted P results in a reduction in both J_{0E} and sheet resistance as indicated by the blue lines in Fig. 7, where each blue line represents a different phosphorus dose. This process trajectory is somewhat orthogonal to the typical $POCl_3$ diffusion.

An additional process advantage of ion-implanted phosphorus emitters is that an in situ passivating oxide can be rapidly grown during the anneal. Bhosle et al. [37] have shown a +0.35% absolute efficiency gain by utilizing an in situ oxide. The high surface concentrations of phosphorus accelerate oxide growth and allow for thicker oxides in short periods of time [38].

The final profile of the cell can be finely tailored by a combination of implant dose and energy, as well as anneal time, temperature and ambient. Fig. 8 summarizes the main parameters of the implant and anneal which control the various portions of the final P profile. Notice that, even after the anneal, the near-surface dose is largely controlled by the initial implant dose and energy. As discussed earlier, it is vital to optimize and control this near-surface P to achieve the best balance of contact resistance to the surface metallization and the highest V_{oc} and J_{sc}.

Performing such an optimization in an industrial line results in a higher efficiency than typical $POCl_3$ diffusion is capable of. This has been demonstrated by Rohatgi et al. [13], who showed an increase in absolute efficiency of +0.3% to +0.8%, and by Wang et al. [39], who showed an improvement in absolute efficiency of more than 0.4%

over $POCl_3$. In cooperation with China Sunergy, Intevac, using their ENERG*i* ion implantation tool, compared implanted cells with standard $POCl_3$ cells processed on a China Sunergy industrial process line [14]. The normalized histogram shown in Fig. 9 already shows a clear improvement using ion implantation with only preliminary optimization. Intevac recently fabricated cells on an industrial manufacturing line with another partner and demonstrated average cell efficiencies exceeding 19.1% (n>2000 wafers). This result also represented a significant improvement over the cell efficiencies for standard $POCl_3$ diffusion. The basic process steps are shown in Fig. 10.

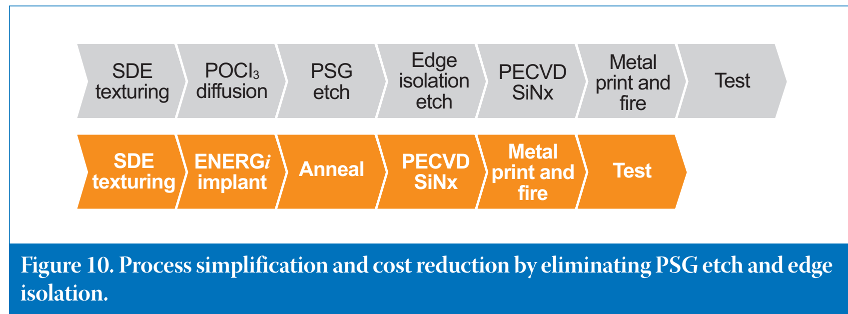

Figure 10. Process simplification and cost reduction by eliminating PSG etch and edge isolation.

Economics

The COO of the recent commercial high-throughput ion implanters is compelling because not only are higher cell efficiencies obtained, but also the distribution of the cell efficiency is narrower. Owing to its high throughput, the ENERG*i* ion implantation tool is cost competitive with the standard $POCl_3$ process via the higher final cell efficiencies and the cost reduction by the elimination of PSG etch and edge isolation.

After process optimization, the ENERG*i* phosphorus implant operating at 2400wph can conservatively improve the cell efficiency by more than 0.5% absolute over the diffusion process. The impact of this on the output of a manufacturing line is an increase of more than 2MWp/year with a value of $1.4 million/year. Narrowing the distribution in cell efficiencies can increase the value even more by virtue of a reduction in scrap, and higher module prices at the higher efficiencies. The investment in the line is also minimized by the fact that adding ion implantation removes the need for wet-etching steps (phosphorus glass etch and edge isolation). This elimination removes approximately $1 million of capital cost from the line and also removes the acid and water running costs (~$0.3 million/year). With these considerations, the payback time of an ion implantation system running at 2400wph is approximately 1.3 years. This is one of the most efficient payback schedules possible in the solar manufacturing business today. The payback time is even shorter for boron implant with higher cell efficiency improvements. As this value is realized, ion implantation systems will become ubiquitous and highly valued by today's Tier 1 solar cell and module manufacturers. Lastly, the Intevac ENERG*i* tool has a very small footprint compared with other tools which handle similar throughput of wafers on the fab line (Fig. 11). This makes retrofitting existing lines for phosphorus implantation easier.

Figure 11. View of the Intevac ENERG*i* ion implantation tool: the actual implantation section is the size of a small minivan.

Conclusion

In the solar cell technology roadmap a transition is taking place in which diffusion processes that have been used for many years are now being replaced by new, cell-efficiency-enhancing ion implantation solutions. Ion implantation offers solar cell manufacturers the capability to extend cell efficiency beyond 19% with a narrower cell efficiency distribution. Additionally, ion implantation offers a path towards the commercialization of new advanced cell architectures, n-type material and IBC cells. A continuous-flux plasma-based ion implantation solution provides the necessary economic solution to achieving this with a very efficient payback schedule.

References

[1] Fischer, M., Metz, A. & Raithel, S. 2012, "Semi international technology roadmap for photovoltaics (ITRPV) – Challenges in C-Si technology for suppliers and manufacturers", *Proc. 27th EU PVSEC*, Frankfurt, Germany.

[2] King, W.J. & Burrill, J.T. 1964, "Solar cells produced by ion implantation doping", *Proc. 4th IEEE PVSC*, Cleveland, Ohio, USA.

[3] Wichner, R. & Charlson, E.J. 1976, "Silicon solar cells produced by corona discharge", *J. Electron. Mater.*, Vol. 5, pp. 513–529.

[4] Ponpon, J. & Siffert, P. 1975, "Silicon solar cells made by ion implantation and glow discharge", *Proc. 11th PVSC*, Scottsdale, Arizona, USA, pp. 342–348.

[5] Muller, J. & Siffert, P. 1981, "Low cost molecular ion implantation equipment", *Nucl. Instr. Meth. Phys. Res.*, Vol. 189, pp. 205–210.

[6] Muller, J. et al. 1985, "Multiple-beam ion implantation setup for large scale treatment of semiconductors", *Nucl. Instr. Meth. Phys. Res. B*, Vol. 6, pp. 394–398.

[7] Tahara Y. et al. 1985, "High throughput automated junction formation by ion implantation and halogen lamp anneal for 9MW production", *Proc. 18th PVSC*, Las Vegas, Nevada, USA, pp. 792–796.

[8] Spitzer, M., Tobin, S. & Keavney, C. 1984, "High-efficiency ion-implanted silicon solar cells", *IEEE Trans. Electron Dev.*, Vol. 31, pp. 546–550.

[9] Spitzer, M. & Keavney, C. 1985, "Low recombination p (+) and n (+) regions for high performance silicon solar cells", *Proc. 18th PVSC*, Las Vegas, Nevada, USA, pp. 43–49.

[10] Spitzer, M. & Keavney, C. 1985, "Attainment of transparent boron-implanted layers for silicon solar cell applications", *Appl. Phys. Lett.*, Vol.

47, pp. 731.
[11] Wood, R., Westbrook, R. & Jellison, G. 1987, "Excimer laser-processed oxide-passivated silicon solar cells of 19.5-percent efficiency", *IEEE Electron Dev. Lett.*, Vol. 8, pp. 249–251.
[12] Yelundur, V. et al. 2011, "First implementation of ion implantation to produce commercial silicon solar cells", *Proc. 26th EU PVSEC*, Hamburg, Germany, pp. 831–834.
[13] Rohatgi, A. et al. 2012, "High-throughput ion-implantation for low-cost high-efficiency silicon solar cells", *Energy Procedia*, Vol. 15, pp. 10–19.
[14] Hieslmair, H. et al. 2012, "High productivity ion implantation for 19% efficient industrial silicon solar cells", *Proc. 27th EU PVSEC*, Frankfurt, Germany.
[15] Dubé, C. et al. 2011, "High efficiency selective emitter cells using patterned ion implantation", *Energy Procedia*, Vol. 8, pp. 706–711.
[16] Jeon, M. et al. 2011, "Ion implanted crystalline silicon solar cells with blanket and selective emitter", *Mater. Sci. & Engineering B*, Vol. 176, No. 16, pp. 1285–1290.
[17] Benick, J. et al. 2012, "Fully implanted n-type PERT solar cells", *Proc. 27th EU PVSEC*, Frankfurt, Germany.
[18] Allebé, C. et al. 2010, "Process integration towards PERL structure", *Proc. 25th EU PVSEC*, Valencia, Spain.
[19] Hermle, M. et al. 2011, "N-type silicon solar cells with implanted emitter", *Proc. 26th EU PVSEC*, Hamburg, Germany.
[20] Meier, D.L. et al. 2011, "N-type, ion-implanted silicon solar cells and modules", *IEEE J. Photovolt.*, pp. 123–129.
[21] Sheoran, M. et al. 2012, "Ion-implant doped large-area n-type Czochralski high-efficiency industrial solar cells", *Proc. 38th IEEE PVSC*, Austin, Texas, USA.
[22] Ok, Y.W. et al. 2012, "Ion-implanted and screen-printed large area 19.6% efficient n-type bifacial Si solar cell", *Proc. 38th IEEE PVSC*, Austin, Texas, USA.
[23] Robbelein, J. et al. 2010, "Towards advanced back surface fields by boron implantation on p-type interdigitated back junction solar cells", *Proc. 25th EU PVSEC*, Valencia, Spain.
[24] Bateman, N. et al. 2012, "High quality ion implanted boron emitters in an interdigitated back contact solar cell with 20% efficiency", *Energy Procedia*, Vol. 8, pp. 509–514.
[25] Grohe, A. et al. 2012, "High-efficient ion implanted back contact cells for industrial application", *Proc. 27th EU PVSEC*, Frankfurt, Germany.
[26] Pelaz, L., Marqués, L.A. & Barbolla, J. 2004, "Ion-beam-induced amorphization and recrystallization in silicon", *J. Appl. Phys.*, Vol. 96, p. 5947.
[27] Collart, E.J.H. et al. 2010, "Process characterization of low temperature ion implantation using ribbon beam and spot beam on the AIBT iPulsar high current", *Proc. 18th Int. Conf. Ion Implant. Tech. IIT 2010*, Kyoto, Japan, pp. 49–52.
[28] Lopez, P. et al. 2005, "Amorphous layer depth dependence on implant parameters during Si self-implantation", *Mater. Sci. & Eng. B*, Vol. 124, pp. 379–382.
[29] Priolo, F. & Rimini, E. 1990, "Ion-beam-induced epitaxial crystallization and amorphization in silicon", *Mater. Sci. Rep.*, Vol. 5, pp. 321–379.
[30] Williams, J. 1983, "Solid phase epitaxial regrowth phenomena in silicon", *Nucl. Instr. Meth. Phys. Res.*, Vol. 209, pp. 219–228.
[31] Suzuki, K. & Tashiro, H. 2003, "High activation of Sb during solid-phase epitaxy and deactivation during subsequent thermal process", *IEEE Trans. Electron Dev.*, Vol. 50, p. 1753.
[32] Pawlak, B. et al. 2012, "Studies of implanted boron emitters for solar cell applications", *Prog. Photovolt.: Res. Appl.*, Vol. 20, pp. 106–110.
[33] Veschetti, Y. et al. 2011, "N-type boron emitter solar cells with implantation industrial process", *Proc. 37th IEEE PVSC*, Seattle, Washington, USA.
[34] Benick, J., Bateman, N. & Hermle, M. 2010, "Very low emitter saturation current densities on ion implanted boron emitters", *Proc. 25th EU PVSEC*, Valencia, Spain, pp. 1169–1173.
[35] Schroder, D.K. & Meier, D.L. 1984, "Solar cell contact resistance – review", *IEEE Trans. Electron Dev.*, Vol. 31, pp. 637–647.
[36] Book, F. et al. 2010, "The etchback selective emitter technology and its application to multicrystalline silicon", *Proc. 35th IEEE PVSC*, Honolulu, Hawaii, USA.
[37] Bhosle, V. et al. 2012, "Value of thermal oxide for ion implant based c-Si solar cells", *Proc. 38th IEEE PVSC*, Austin, Texas, USA, pp. 002128–002131.
[38] Ho, C. & Plummer, J. 1979, "Si/SiO interface oxidation kinetics: A physical model for the influence of high substrate doping levels", *J. Electrochem. Soc.*, Vol. 126, p. 1516.
[39] Wang, X.-S., Li, Y.-M. & Zhang, L.-J. 2012, "Over 19% CE c-Si cells enabled by ion implantation", *Proc. 27th EU PVSEC*, Frankfurt, Germany.

About the Authors

Dr. Henry Hieslmair is currently Principal Solar Scientist at Intevac, managing tool design and processes for ENERG*i* ion implantation for solar cells. With 20 years' experience in the silicon solar field, he has researched a wide range of topics from basic defects in silicon materials to developing an entirely laser-doped IBC on thin silicon. Henry holds numerous patents and has published over 40 papers in solar technology.

Ian Latchford is Senior Director of Solar Product Marketing at Intevac. He has over 25 years' experience of semiconductor and solar technology in management and marketing positions with leading Silicon Valley companies. Ian has a B.S. in chemical engineering from South Bank University, London, and holds a number of semiconductor and solar patents.

Lisa Mandrell is Senior Process Manager at Intevac. With a background of 16 years in the solar industry working in research and development, process transfer and process optimization for manufacturing, Lisa is responsible for the characterization and optimization of ion implantation and supporting processes.

Dr. Moon Chun is Director of Technology at Intevac. He co-invented and designed the beamline for the ENERG*i* implanter and is currently responsible for equipment development for ion implanters. Moon earned his Ph.D. in nuclear engineering and engineering physics at the University of Wisconsin-Madison and his B.S. at the University of California-Berkeley.

Dr. Babak Adibi is VP and GM of the Solar Implant Group at Intevac. Previously, he was President of Solar Implant Technologies, which he co-founded, and before that he was responsible for the successful development and industry adoption of several ion implantation and laser annealing systems for solar and semiconductor applications. Babak is the author of numerous peer-reviewed scientific publications and patents in ion implantation and related fields, holding a Ph.D. in ion implantation, an M.Sc. in nuclear power from Surrey University, and a B.Sc. in physics from Imperial College London.

Enquiries

Intevac
3560 Bassett Street
Santa Clara, CA 95054
USA

Tel: +1 408 986 9888
Email: hhieslmair@intevac.com
Website: www.intevac.com